Levi Benjamin (Orcid ID: 0000-0002-0508-1765)

Short Wave Infrared Light Imaging Measures Tissue Moisture and Distinguishes Superficial from Deep Burns

Sergey Mironov PhD[3]*, Charles D. Hwang BS[2]*, Jean Nemzek DVM MS[5], John Li MD[2], Kavitha Ranganathan MD[1] , Jonathan T. Butts BS[2], David J. Cholok BA[2] , Vladislav A. Dolgachev PhD[2], Stewart C. Wang MD PhD[2], Mark Hemmila MD[2], Paul S. Cederna MD PhD[1], Michael D. Morris PhD[4], Omer Berenfeld PhD[3] **, Benjamin Levi MD[1] **

[1] Department of Plastic Surgery, [2] Department of Surgery, [3] Center for Arrhythmia Research, [4] Department of Chemistry, [5] Unit for Laboratory Animal Medicine, University of Michigan, Ann Arbor, MI, USA

* indicates equal first authorship

** indicates equal senior authorship

Corresponding Author and Address for reprints:

Benjamin Levi, MD
Burn/Wound and Regenerative Medicine Laboratory
1150 W. Medical Center Dr.
Ann Arbor, MI, 48109
Phone: 734-936-0034
Fax: 734-763-6199
Division of Plastic Surgery, Department of Surgery, University of Michigan Health System, 1500 E Medical Center Drive, SPC 5340, Ann Arbor, MI 48109-5340

This is the author manuscript accepted for publication and has undergone full peer review but has not been through the copyediting, typesetting, pagination and proofreading process, which may lead to differences between this version and the Version of Record. Please cite this article as doi: 10.1111/wrr.12779

ABSTRACT

Existing clinical approaches and tools to measure burn tissue destruction are limited resulting in misdiagnosis of injury depth in over 40% of cases. Thus, our objective in this study is to characterize the ability of short wave infrared (SWIR) imaging to detect different moisture levels which could serve as surrogate for tissue viability as well as the ability to differentiate between superficial and deep burns damaging the epidermis and dermis at different depths. To accomplish our aim we constructed an imaging system consisting of a broad-band Tungsten light source, 1200, 1650, 1940 and 2250 nm wavelength filters and a specialized SWIR camera. We initially used agar slabs to provide a baseline spectrum for SWIR light imaging and demonstrated the differential absorbance at the multiple wavelengths, with 1940 nm being the highest absorbed wavelength. The 1940 nm reflected light was then demonstrated to detect levels of moisture in inorganic and *in vivo* mice models. The multi-wavelength SWIR imaging approach was then used to diagnose depth of burns using an *in vivo* porcine burn model. Healthy and injured skin regions were imaged 72 hours after short (20 sec) and long (60 sec) burn application and biopsies were extracted from those regions for histologic analysis. Burn depth analysis based on collagen coagulation histology confirmed the formation of superficial and deep burns. SWIR multi-spectral reflectance imaging showed enhanced intensity levels in long burned regions, which correlated with histology and distinguished between superficial and deep burns. This SWIR imaging method represents a novel, real time method to objectively distinguishing superficial from deep burns.

INTRODUCTION

Thermal injuries represent a significant public health burden given that over 265,000 people die of burn injuries each year. In the United States alone, over 400,000 people receive medical care for burn injuries each year, with over 10% of these injuries requiring hospitalization and surgical intervention[1,2]. In the setting of thermal injury, depth of injury dictates therapy and patient outcomes. It is well known that superficial thickness burns heal well without surgery, while deep, full thickness injuries require prompt debridement and grafting to prevent the adverse sequelae of scar contractures, infections, and delayed wound healing[3-5]. Thus, the crux of decision-making for burn surgeons lies in gauging the necessity of surgical debridement, a determination commonly made within seven days of presentation[6]. The current standard of care relies on clinical judgment and experience, factors that are difficult to appraise critically due to the absence of objective data and standardization[1,2]. Additionally, as burn care is provided by both experienced and inexperienced clinicians, objective diagnostic strategies can improve the triage process for patients in the field in a point of care fashion.

Objective pre- or intra-operative measurements of tissue viability using histology from tissue biopsy are impractical, expensive, invasive, and subject to sampling errors. Additionally, tissue biopsy only provides information at the specific time and site from where the biopsy was taken. Therefore, physical exam is the most commonly utilized method to evaluate depth of injury. Importantly, clinician judgment regarding the need for intervention correlates to objective measures of tissue viability only 60% of the time. Consequently, patients undergo either

disproportionately more or less surgery than what is appropriate 40% of the time leading to longer hospital stays and poorer outcomes[1,7,8]. Thus, an objective and practical method of measuring the depth of tissue injury has the potential to augment currently available diagnostic modalities.

Methods for better imaging strategies to evaluate tissue viability and guide the need for surgical debridement are necessary and short wave infrared spectroscopy (SWIR) has been proposed as a potential solution[9-12]. Light in the SWIR spectrum, defined as wavelengths between about 1000 and 2500 nm (Figure 1A), contains absorption peaks for O-H bonds (1430 and 1940 nm), lipid-associated C-H absorption peaks (1210, 1730, and 1760 nm) and collagen (1200 and 1500 nm). Thus, measuring the reflectance of light in the SWIR range was proposed for measurement of moisture.[12] We further surmise that the SWIR light reflectance sensitivity to tissue factors and moisture could also make it an important marker of skin tissue viability in burns, as suggested by the conjunction between water loss and epidermal barrier dysfunction[13-15]. Previous literature, especially in dermatologic journals, have characterized the composition of healthy cutaneous tissues. Namely, strong water signals have been characterized within the stratum corneum and viable epidermis[13]. Furthermore, studies investigating compositional changes after mechanical damage to the cutaneous layer have demonstrated increases in transepidermal water loss i.e. decrease in moisture content[14,15]. Thus, in Figure 1B we illustrate the derived postulate that in viable skin that is well-hydrated, increased water content preferentially attenuates the reflectance of the 1940 nm wavelength compared to the 1650 nm or 1200 nm. However, in full-thickness burns, damage to vasculature and sebaceous glands renders the tissue less hydrated and

it is hypothesized to increase reflectance intensity across the whole SWIR spectrum. Therefore, the goal of the current study is to evaluate the ability of SWIR imaging to distinguish between burns of different depth. To this end, we applied the SWIR light imaging to inert compounds with variable thicknesses and moisture levels, and ultimately to an *in vivo* porcine thermal skin injury model.

METHODS

Ethics Statement

All animal experiments described were approved by the Institutional Animal Care and Use Committee at the University of Michigan, Ann Arbor. This study was carried out in strict accordance with the recommendations in the Guide for the Care and Use of Laboratory Animals of the National Institutes of Health.

The Imaging System and Procedures

The Short Wave Infrared (SWIR) imaging system consisted of three components: (i) a custom made broadband DC 0.5 kW collimated tungsten-filament light source, (ii) Filters centered at 1200, 1650, 1940 and 2250 nm and ±10 nm width (Thorlabs). The filters were either mounted on a filter-wheel attached to the light source or attached to the camera; and (iii) a SWIR camera (Xeva-2.35-320, Xenics, Leuven Belgium) with a type 2 strained sensor layer (T2SL) sensitive in the 1-2.35 μm wavelengths range. Images of targets were acquired and processed with the software provided with the SWIR camera (Xeneth v2.6, Xenics, Leuven, Belgium). Images of 320×256 14-bit pixels were collected as 100 frames videos at 15 frames per second with integration time between 12 and 30 msec. Camera output yielded pixels intensity values in Analog to Digital converter Units (ADU). Recorded images were processed before analysis with a factory-supplied filter compensating for aberrant pixel values and fixed pattern noise of the imaging sensor. All SWIR readings were conducted in procedures space with controlled temperature (23 °C) and relative humidity (40-50 %) in accordance with animal care guidelines.

Agar Preparation for Baseline SWIR Characteristics

Agar is a heterogeneous mixture of two classes of polysaccharide polymer derived from seaweed and used to cast gel layers in skin phantom model slabs[16]. Baseline SWIR imaging was performed on agar slabs. Slabs using 1 g agar (Sigma Aldrich Corporation, USA) mixed into 30 ml water were constructed in petri dishes (ThermoFisher Scientific, USA) as 2D layers with 1, 2, 3, 5 and 10 mm thickness. The petri dishes were then placed in two different configurations for illumination and imaging as schematically described in Figure 2A. In the Epi-illumination (left panel) configuration the petri dish is illuminated and imaged from the same side such that the light is traversing the slab twice. In the Trans-illumination configuration (right panel), the illumination and the imaging is at opposing sides of the slab such that the light is traversing the slab only once. For scaling of absorbance, images were also obtained with empty petri dishes equivalent to zero thickness slabs.

Baseline Moisture Models

To ensure that the SWIR imaging system detected variation in moisture levels we performed three tests. The light source and SWIR camera were placed about 20 cm from the imaged surfaces in an Epi-illumination configuration. A 25-cm diameter P8 grade filter paper (Fisherbrand, Fisher Scientific, Pittsburgh, PA) was applied with 50 μL distilled water at room temperature and imaged at 1200, 1650, 1940 and 2250 nm simultaneously across the dry and wet regions. Additionally, light reflectance at 1940 nm, which is a water characteristic O-H bond absorption peak[17], was imaged from Kimwipe (Kimtech Science Brand; Roswell, Georgia)

measuring 4.4×8.4 inches sequentially before and after application of 30 μL of distilled water at room temperature. To evaluate the ability of SWIR imaging to detect different levels of moisture *in vivo*, we also applied no water, 10, 20, and 30 μL of distilled water to the dorsum of 3 male C57BL/6 mice of 6 weeks of age (Charles River, Wilmington, MA). Mice were anesthetized using inhaled 1-3% isoflurane, and euthanized with CO_2 overdose upon completion of the procedure.

Porcine Burn Model

The porcine burn model was adapted from the protocol previously described by Singer *et al*[18]. Five female Yorkshire-cross pigs (Michigan State University Swine Research, East Lansing, MI) weighing 30-35 kg were singly housed with access to water and enrichment and allowed to acclimate to the facilities for at least 7 days prior to the procedures. On the day of a procedure, each pig was sedated with telazol (2.0-8.0 mg/kg IM, Zoetis, Kalamazoo, MI) and xylazine (1.0-3.0 mg/kg IM, AnaSed, Akorn, Decatur, IL). Anesthesia was maintained using 1-4 % isoflurane in 100% oxygen delivered by mask. Prior to the burn injury, the pigs were given an intramuscular injection of 0.05 mg/kg buprenorphine and transdermal buprenorphine patches (total dose of 30 μg/hr, Butrans, Purdue Pharma, Stamford, CT) were applied at the dorsal base of the neck. Animals were euthanized with an overdose of pentobarbital given in the ear vein upon completion of the procedures.

Following anesthesia, the animal's dorsal skin was prepped by chemically removing all hair with Nair for 8-10 minutes followed by a wash with warm water. The skin was then disinfected with three alternating scrubs of chlorhexidine and alcohol, which was allowed to dry. Using a, 150

g copper block with an area of 5×5 cm^2 and heated in a hot water bath (80 °C) before each application, up to 4 burns were created by applying the block to the dorsum of the pig for 20 sec (referred to as short duration burns) and additional up to 4 burns deeper burns by applying the heated block for 60 sec (referred to as long duration burns). The burn regions were 2 cm lateral to the dorsal midline and at least 2 cm apart from one another to ensure independency from the adjacent zone of thermal injury. The burn sites were bandaged with Telfa (Medline, Mundelein, IL) and Tegaderm (3M, St Paul, MN). Cotton padding was placed over the bandaged burns and the pigs were -wrapped loosely with Coban (3M, St Paul, MN) from thorax to abdomen, then covered with a cotton jacket. Dressings were changed daily using the anesthesia protocol outlined above. Animals were also anesthetized to facilitate image acquisition and punch biopsies for histological analysis.

Short wave infrared (SWIR) imaging of pigs' burns was performed 72 hr after the burns were created. Light source and SWIR camera were set in Epi-Illumination configuration affixed to a mobile cart, ensuring a fixed angle of about 30 deg between optical axes of camera and incident light. Camera was positioned normal to the preparations surface at a distance of about 20 cm. Each burn site was imaged individually along with 2 flanking control regions from an unburned area of nearby skin. SWIR images of reflectance from a template uniform background (Figure 2) were used as a normalizing reference for the distribution of illumination intensity in space. Areas of 50×50 pixels (~5×5 mm^2) at the center of each region of interest, excluding burn edges and biopsy sites, were used to determine average intensity values.

Histological Analysis

Full burn thickness punch biopsies (4 mm diameter) were acquired at the time of anesthesia from the porcine skin. The tissue specimens were fixed in 10 % buffered formalin for 24 hr at 4 °C and dehydrated in serial preparations of ethanol. In order to accurately assess the depth of the burns, specimens were embedded in paraffin (Leica EG1150 C, Leica, Wetzlar, Germany) and sectioned into 5 μM thick longitudinal slices (Leica RM2255, Leica, Wetzlar, Germany). Sections were then deparaffinized, rehydrated, and stained with H&E and Picrosirius red[19]. Analysis for burn depth was primarily based on collagen alteration depth as determined by hyaline changes and seroproteinaceous infiltrate[20,21]. Depth of injury was determined within specimens by measuring the length from the outer edge of the epidermis layer to the level of the deepest area of collagen coagulation. All images were manually segmented in FIJI/ImageJ to circumscribe the entire region of the burn and calculate average depth. Segmentations were performed by three blinded analyzers previously trained by a board certified clinical pathologist's practice set.

Statistical Analysis

Animal imaging and histology data are confirmed to be normally distributed with Shapiro-Wilk test and are reported as mean ± standard deviations, except where noted. One-sided or two-sided student's t-tests were used to show significant difference between imaged and histology groups, respectively. Weighted linear regression analysis was performed on moisture imaging. Levene's (homoscedasticity) test was applied to porcine histology analysis. 2-way ANOVA was

applied to porcine spectral imaging of burns of various durations. For each test, p less than 0.05 is considered significant.

RESULTS

Basic SWIR Light Imaging Characteristics

For basic characterization of SWIR light absorption and reflection in a biological phantom model we performed a well-controlled Epi- and Trans-illumination imaging experiments on agar slices of variable thicknesses[16]. Figure 2A shows the imaging setups (see Methods) and Figure 2B describes the dependence of the absorbance fraction on the thickness of the agar slabs. The absorbance fraction was calculated as the space averaged ratio of intensity without agar minus the intensity with agar to the intensity without agar. The absorption fraction graphs show approximately similar relative dependency for Epi- and Trans-illumination imaging for all wavelengths. It is seen that the 1200, 1650 and 2250 nm light is gradually and monotonically more absorbed by slabs with increasing thicknesses between 1 and 5 mm regardless of the Epi-and Trans-illumination settings. The data also show that for both illumination configurations our light sources and camera system is not capable to determine the agar slab thickness by the 1940 nm light because that light is almost entirely absorbed already by a 1 mm thickness slab. The information from this test suggests that the 1650 nm light is absorbed in agar more than 1200 and 2250 nm light. It is also suggested that the 1940 nm light should be used mainly for sub-millimeter surface-most skin layer analyses and that the 1200 and 2250 nm light could be used for deeper skin layers analyses.

SWIR Light Imaging Delineates Moisture Content

A baseline demonstration of water effect on SWIR reflectance is demonstrated in Figure 3A. White paper was wetted with 50 μL distilled water and then the dry and wetted regions were imaged with the Xeva-2.35-320 camera under collimated tungsten Epi-illumination at 1200, 1650 1940 and 2250 nm light. Images (top) show a central dark spot corresponding to the wet region. A profile of light intensity across the dry and wet regions (red line) demonstrates that the relative reflectance of the moist regions in this setup was less than the surrounding dry regions. Notably the reflectance at 1940 nm was the lowest among all 4 wavelengths at 50 % in the wetted relative to the dry regions. Following, the effect of water on reflectance was quantified at the 1940 nm sequentially in the same region before and after application of 30 μL of water. Reflectance intensity wavelength was significantly less in the wet region compared to dry region with a mean difference between dry and wet regions of the paper measuring 635 ADU ($p<0.0001$; panels A and B in Figure 3). Taken together, panels A and B demonstrate that regional water application is detectable using our SWIR, mainly 1940 nm, Epi-illumination imaging approach. Similar differences between moist and dry tissue were noted when varying degrees of water were applied topically to the dorsum of a mouse (Panel C in Figure 3). In this model, there was a significant decrease in spectral intensity in moist skin compared to dry skin after application of 10, 20, and 30 μL water. Cumulative data from 3 mice shown in Panel D demonstrates a monotonic decreased in averaged 1940 nm reflectance intensity with increasing amounts of applied water (in ADU): 794±83, 444±73, 334±90 and 235±43 for 0, 10, 20 and 30 μL water, respectively ($p<0.05$ between all groups comparisons). A weighted linear regression analysis of the data in Figure 3D yielded

R=0.953 (Adjusted R-Square=0.863 and p=0.047) and confirmed that light reflectance at 1940 nm is sensitive to water content[12].

SWIR Light Imaging and Depth of Damaged Tissue in a Porcine Burn Model

Next we used a clinically relevant porcine model to study spectral SWIR light reflectance in deep and superficial burns. Figure 4A shows a total of 8 burn regions in a sample animal: In each animal, up to 4 short (S) and 4 long (L) duration contact with a heated metal block were applied in the demarcated dorsal regions with unburned surrounding area. At 48 hr post burn, biopsies from the burned regions were excised and at 72 hr post burn, the burn and unburned regions were imaged with the spectral SWIR. Figure 4B shows 4 unprocessed SWIR images from sample short (top) and long (bottom) duration burn regions. The images demonstrate heterogeneous reflectance with heterogeneous demarcation of the short (pink arrow) and long (red arrow) heat application regions and whereby overall reflectance intensity at 1200 and 2250 nm is visibly higher than at 1650 and 1940 nm. In Panel C of Figure 4, the unprocessed images of Panel B were processed to differentiate between the short and long duration burn regions. The processing consisted of summing the 1650 and 2250 nm images and normalization by the 1940 nm image to account for non-uniform illumination. The resulted images show pixels in the short burn (top) are darker than in the long burn (middle), which is further illustrated by an image of the difference in their pixels values (L –S, bottom) showing more white pixels in the burned regions and black pixels in the surrounding area.

To quantify the general ability of the SWIR imaging to distinguish between burn regions we processed a total of n=17 short and n=17 long duration heated regions, along with nearby unburned regions, imaged at the 4 separated wavelengths. The processing of the images for reflectance fraction of each individual region and wavelength included normalizing the images with the corresponding spectral images of reflectance from a reference surface to account for the non-uniform illumination (see Methods). The cumulative reflectance fractions for all the regions and all wavelengths are shown in Figure 4D. A 2-way ANOVA analysis on the data from the 5 animals reveals that reflected fraction is different for both each wavelength ($p<0.001$) and for each treatment (i.e., unburned, short and long duration heating, $p=0.011$). As shown in the graph, imaged wavelengths of 1200, 1650 and 2250, but not 1940 nm, show a significant 10-20 % higher averaged reflectance in the long duration burn in comparison to the unburned region. The insensitivity of the 1940 nm reflectance to the burns is consistent with the insensitivity of that wavelength to agar thickness shown in Figure 2B. Notably, the 1650 and 2250 nm reflectance intensity from long duration heating regions was 10-20 % higher while the 1940 nm reflectance is not significantly different from the short duration heating regions, which explains the processing of images at those wavelengths to distinguish between the sample short and long burns illustrated in Figure 4C.

In addition to the SWIR imaging, biopsies where taken from the edges and center of the burned regions for histology analysis as shown in Panel B (green arrows). Figure 4E shows sample H&E and Picrosirius red stained sections from short (left) and long (right) burns duration biopsies.

The superimposed outlined edges of collagen alteration[20,21] used as a marker for burn depth corroborates the deeper dermis incurred damage in tissue under heating. The graph in Figure 4E analyzes 10 sampled biopsies in each treatment region and finds that on average the long duration heating damages tissue as deep as 922±45 μm while the short duration heating damages tissue 590±57 μm deep ($p<0.001$). Taken together, the data presented in Figure 4 shows that we have generated a deep and superficial dermis burned regions in the porcine model and that SWIR imaging at specific wavelengths of 1650 and 2250 nm can distinguish between these two regions.

DISCUSSION

Our study aimed at demonstrating the conceptual utility of short wave infrared (SWIR, ~1000-2500 nm) imaging in diagnosing the depth of viable tissue in skin burns. We have demonstrated that specific wavelengths of the SWIR light range are sensitive to tissue moisture in mice and distinguish between superficial and deep burn injury in porcine.

Models of Skin Burns

Papp et al (2004)[21] previously validated a reproducible model of pig burn for histological analysis of burn depth. While the authors were able to demonstrate reliability and reproducibility of their model, their deeper burns all converged to a deep burn depth. In order to produce a more tunable model, we performed our inductive burns with cooler blocks and for longer contact times (20° C cooler, and ×2-4 longer, respectively). Meyerholz et al (2009)[20] previously characterized parameters to determine burn depth via histology in an acute rat model, demonstrating a linear relation between contact time and average depth. Although their study's biopsies were performed at 5 hours, extrapolating their dose-dependency linear regression on burn depth is consistent with our porcine model that remained stable to the day 3 time point (not shown). This resolution affords advantages in the validation of separate diagnostic modalities and characterization of treatment effects in a burned skin model that resembles human tissues.

SWIR Light and Imaging of Biological Tissue

The benefit of imaging skin burns in the SWIR spectrum lies in the ability of light in this range to penetrate tissue deeper than light in the visible and near-infrared spectrum, while limiting

penetration to avoid confounding deep tissue edema, as occurs in mid-infrared light. Additionally, the presence of resonance wavelengths for O-H and C-O vibrational overtone in this region of the SWIR light detects compounds such as collagen, lipid, and water with greater sensitivity than near-infrared imaging or other modalities. Moisture levels, a tissue quality commonly evaluated by burn surgeons to gauge the depth of tissue injury, are best captured in the SWIR spectrum, with signal absorbance at 1940 nm that is 260 fold greater than at 970 nm in the near-infrared spectrum[22]. Nevertheless, variability in skin conditions and imaging methods hamper comparisons of water absorbance of SWIR light between different studies[23]. Furthermore, the need for a consistent electrical contact with the skin surface as well as an exquisite sensitivity to ambient temperature render also electrical measurements for assessment of trans-epidermal water loss, such as capacitance, as non-adequate for comparisons with our imaging results[13,15].

In this study, we demonstrate that SWIR imaging at certain wavelengths detects differences in moisture and differentiates superficial from deep burns in a non-invasive fashion using an *in vivo* porcine model with histology as the gold standard for comparison. These distinctions, while binary and not yet representative of the clinical spectrum of burn depths encountered, suggests a future role for SWIR imaging in determining viability of tissue in the acute setting. The moisture imaging data shown in Figure 3 is consistent with the ability of 1940 nm reflectance to detect moisture levels *in vivo* amounts of <30 μL, but the relation of 1940 nm light reflectance to burn depth has not been fully established as our imaging analysis in the agar slabs of >1 mm in thickness (Figure 2) and burns with damaged collagen at depth between about 0.5-1 mm (Figure 4) show

similar levels of absorbance or reflectance of 1940 nm light. Further investigation is required to clarify the effect of water content at different skin depths on the SWIR light reflectance[13-15].

Our 2-way ANOVA of the burns images demonstrated that the SWIR reflectance depends on both the wavelengths of the images and the burn depths. In general, the combined analysis of reflectance-sensitive wavelengths could enhance the burn depth discrimination, while a reflectance that is indifferent to the physiological underlying conditions of the substrate could be used for calibration purposes. Accordingly, in this study we utilized sample burns images captured at 1940 nm, who showed no significant reflectance sensitivity to the skin conditions (Figure 4D), to normalize the images captured at 1650 and 2250 nm. As illustrated in Figure 4C, the panels of the normalized images augmented the visual impact of the images in Figure 4B, who showed a modest 10-20 % reflectance differences (Figure 4D), and enabled a clearer distinction between the unburned, the short and the long burn regions. Future research following the concepts utilized here may identify other SWIR wavelengths and processing for a better analysis of different burn depths.

Our results agree with those of previous studies that indicate the benefit of SWIR technology. SWIR optical sensing of skin has been previously used to characterize porcine and human skin[12,24,25]. However, these measurements have been performed *ex-vivo*, with a limited SWIR range and have not been used to assess burns or traumatic wounds. SWIR has also been used to identify atherosclerotic plaque and stages of malignancy in breast cancer[26,27]. The non-invasive method of measuring the composition and nature of deeper anatomic structures is critically important to the overarching benefit of SWIR imaging. SWIR imaging is currently used

to quantify skin moisture after application of topical facial cosmetics[11,12], however SWIR imaging has not been tested in the past with regards to its efficacy in the setting of thermal injury.

Clinical Management of Burns

The current standard of care for thermal injury is debridement to viable tissue layers, however, the precise plane of transition is difficult to determine across an injury and under or over debridement ultimately lead to increased patient morbidity[1,7,8]. We propose that use of our non-invasive point of care SWIR imaging modality will allow clinicians to more clearly diagnose superficial versus deep burns based on surface moisture and tissue viability as the key variables of interest guiding the treatment toward excision or non-surgical management. This modality, like a conventional visible light point and shoot camera, does not contact the patient and does not require the injection of fluorescent markers[22]. Given short, efficient acquisition times, the development of a novel, accurate, non-contact, rapid, and portable point of care technology for use in military, veteran, and civilian patients will allow for a more objective assessment of burn wound depth.

Although technologies have been developed to facilitate burn injuries management including determination of viability, currently available modalities, including LDI, ICG video angiography and NIR imaging, have important limitations that have restricted the potential for standardized clinical use in military, veteran, and civilian populations[22]. While new technologies have recently come forth to define burn depth, these modalities have important limitations that restrict their potential for standardized clinical use[28]. Laser Doppler imaging (LDI) measures the volumetric flux of blood at a site to determine tissue viability. While studies have demonstrated

greater than 95 % correlation between histology and LDI in terms of accuracy of determining tissue viability, this method requires large instrumentation that is not portable and can be very expensive. Most importantly, however, LDI is only able to be used within the narrow window of 2-5 days after injury, and is not recommended for use in patients with comorbidities such as anemia, cellulitis, or vascular disease[29,30]. Thus, clinical applicability is severely limited as a result of these restrictions. ICG videoangiography is another modality of macroimaging used to visualize the patency of vasculature within the deep dermis. Using this system, patients receive an intravenous injection of indocyanine green. Tissues that are viable demonstrate high uptake of indocyanine green, while tissues that are less viable demonstrate lower uptake visualized as lower fluorescence. The main limitation of this modality is the need for intravascular injection, an invasive procedure that is difficult to repeat and can result in pain, anaphylaxis, headache, and urticaria[29]. Another example of a technology that has demonstrated limited clinical adoption is near infrared (NIR) imaging. Although this device visualizes burn wound edema as a metric of tissue injury, the particular wavelength used is only able to evaluate the quality of deeper tissues and not the more superficial tissues that require debridement[9,22,31]. Furthermore, NIR is not able to reliably and reproducibly evaluate surface moisture, which is the primary region of interest with our new system. Finally, both NIR and LDI depend on blood flow; thus, burn debridement performed on extremities under tourniquet preclude use of these technologies.

Limitations

There are important limitations to consider. First, our analysis is a proof of concept validation of the feasibility of SWIR imaging in determining the extent of burn injury, but it is not yet correlated to differences in clinical outcomes. Second, our study was conducted in only 2 burn depths and we do not have sufficient spatial resolution in biopsies for histological data to support the fine spatial details that represent all pathological conditions that may affect light reflectance. Furthermore, our burn study was performed at 72 hr post injury and did not perform long-term follow up of burned specimens and debridement based on the SWIR readings. Finally, although the porcine thermal injury model has been extensively validated, intrinsic differences to human skin necessitate additional studies to assess the efficacy of SWIR systems in human patients[32].

Conclusions

Objective measures of burn wound depth are important to properly diagnose and treat patients with burns. Our study in mice and porcine models suggests that SWIR imaging can detect skin moisture and can distinguish between superficial and deep burns under certain conditions. Thus SWIR imaging and metrics may represent a new non-invasive technology to guide tissue debridement. Once validated in humans, SWIR technology will add objective data to supplement pre-existing clinical standards of care.

Acknowledgements

The authors would like to thank the staff at the University of Michigan Microscopy and Imaging Laboratory (MIL) for their assistance.

Source of funding

This study was supported in part by the Coulter Translational Research Partnership Program at the University of Michigan (BL, OB), NIH/National Institute of General Medical Sciences Grant K08GM109105-0, NIH R01GM123069, ACS Clowes Award, Department of Defense W81XWH-18-2-0038 (BL), Department of Defense/US Army W81XWH-16-1-0574 (JN), NIH/National Heart, Lung, and Blood Institute R01-HL118304 (SM, OB), and Research Grants from Medtronic, Inc., and Abbott (SM, OB).

Conflict of Interest

OB: In portions of time during the performance of this study he was a cofounder and Scientific Officer of Rhythm Solutions, Inc., Research and Development Director for S.A.S. Volta Medical and consultant to Acutus Medical. Also received Honoraria from Aurora Medical, Biosence-Webster and Boston Scientific. None of these activities is related to the present study.

REFERENCES

1. Sen CK, Gordillo GM, Roy S, et al. Human skin wounds: a major and snowballing threat to public health and the economy. *Wound repair and regeneration : official publication of the Wound Healing Society [and] the European Tissue Repair Society.* 2009;17(6):763-771.
2. Kauvar DS, Wolf SE, Wade CE, Cancio LC, Renz EM, Holcomb JB. Burns sustained in combat explosions in Operations Iraqi and Enduring Freedom (OIF/OEF explosion burns). *Burns : journal of the International Society for Burn Injuries.* 2006;32(7):853-857.
3. D'Avignon LC, Chung KK, Saffle JR, Renz EM, Cancio LC, Prevention of Combat-Related Infections Guidelines P. Prevention of infections associated with combat-related burn injuries. *The Journal of trauma.* 2011;71(2 Suppl 2):S282-289.
4. Hospenthal DR, Murray CK, Andersen RC, et al. Executive summary: Guidelines for the prevention of infections associated with combat-related injuries: 2011 update: endorsed by the Infectious Diseases Society of America and the Surgical Infection Society. *The Journal of trauma.* 2011;71(2 Suppl 2):S202-209.
5. Levi B, Jayakumar P, Giladi A, et al. Risk factors for the development of heterotopic ossification in seriously burned adults: A National Institute on Disability, Independent Living and Rehabilitation Research burn model system database analysis. *The journal of trauma and acute care surgery.* 2015;79(5):870-876.
6. Saffle JR. Critical Care Management of the Severely Burned Patient. In: Parrillo JE, ed. *Critical Care Medicine*. 4th ed: Saunders; 2014:1177-1198.
7. Loder S, Peterson JR, Agarwal S, et al. Wound healing after thermal injury is improved by fat and adipose-derived stem cell isografts. *Journal of burn care & research : official publication of the American Burn Association.* 2015;36(1):70-76.
8. Heimbach D, Engrav L, Grube B, Marvin J. Burn depth: a review. *World journal of surgery.* 1992;16(1):10-15.
9. Cross KM, Leonardi L, Payette JR, et al. Clinical utilization of near-infrared spectroscopy devices for burn depth assessment. *Wound repair and regeneration : official publication of the Wound Healing Society [and] the European Tissue Repair Society.* 2007;15(3):332-340.
10. Edgar DW, Briffa NK, Cole J, et al. Measurement of acute edema shifts in human burn survivors--the reliability and sensitivity of bioimpedence spectroscopy as an objective clinical measure. *Journal of burn care & research : official publication of the American Burn Association.* 2009;30(5):818-823.
11. Egawa M, Yanai M, Maruyama N, Fukaya Y, Hirao T. Visualization of Water Distribution in the Facial Epidermal Layers of Skin Using High-Sensitivity Near-Infrared (NIR) Imaging. *Applied spectroscopy.* 2015;69(4):481-487.

12. Arimoto H, Egawa M. Imaging wavelength and light penetration depth for water content distribution measurement of skin. *Skin research and technology : official journal of International Society for Bioengineering and the Skin.* 2015;21(1):94-100.
13. Ezerskaia A, Uzunbajakava NE, Puppels GJ, et al. Potential of short-wave infrared spectroscopy for quantitative depth profiling of stratum corneum lipids and water in dermatology. *Biomed Opt Express.* 2018;9(5):2436-2450.
14. Vergou T, Schanzer S, Richter H, et al. Comparison between TEWL and laser scanning microscopy measurements for the in vivo characterization of the human epidermal barrier. *J Biophotonics.* 2012;5(2):152-158.
15. Rosado C, Rodrigues LM. In vivo study of the physiological impact of stratum corneum sampling methods. *Int J Cosmet Sci.* 2003;25(1-2):37-44.
16. Chen AI, Balter ML, Chen MI, et al. Multilayered tissue mimicking skin and vessel phantoms with tunable mechanical, optical, and acoustic properties. *Medical physics.* 2016;43(6):3117-3131.
17. Ali JH, Wang WB, Zevallos M, Alfano RR. Near infrared spectroscopy and imaging to probe differences in water content in normal and cancer human prostate tissues. *Technology in cancer research & treatment.* 2004;3(5):491-497.
18. Singer AJ, Hirth D, McClain SA, Crawford L, Lin F, Clark RA. Validation of a vertical progression porcine burn model. *Journal of burn care & research : official publication of the American Burn Association.* 2011;32(6):638-646.
19. Chvapil M, Speer DP, Owen JA, Chvapil TA. Identification of the depth of burn injury by collagen stainability. *Plastic and reconstructive surgery.* 1984;73(3):438-441.
20. Meyerholz DK, Piester TL, Sokolich JC, Zamba GK, Light TD. Morphological parameters for assessment of burn severity in an acute burn injury rat model. *International journal of experimental pathology.* 2009;90(1):26-33.
21. Papp A, Kiraly K, Harma M, Lahtinen T, Uusaro A, Alhava E. The progression of burn depth in experimental burns: a histological and methodological study. *Burns : journal of the International Society for Burn Injuries.* 2004;30(7):684-690.
22. Wilson RH, Nadeau KP, Jaworski FB, Tromberg BJ, Durkin AJ. Review of short-wave infrared spectroscopy and imaging methods for biological tissue characterization. *Journal of biomedical optics.* 2015;20(3):030901.
23. Bashkatov AN, Genina EA, Kochubey VI, Tuchin VV. Optical properties of human skin, subcutaneous and mucous tissues in the wavelength range from 400 to 2000 nm. *J Phys D Appl Phys.* 2005;38(15):2543-2555.
24. Anthony JC, Anthony TG, Kimball SR, Jefferson LS. Signaling pathways involved in translational control of protein synthesis in skeletal muscle by leucine. *The Journal of nutrition.* 2001;131(3):856S-860S.
25. Edgar MP, Gibson GM, Bowman RW, et al. Simultaneous real-time visible and infrared video with single-pixel detectors. *Scientific reports.* 2015;5:10669.

26. Cerussi A, Shah N, Hsiang D, Durkin A, Butler J, Tromberg BJ. In vivo absorption, scattering, and physiologic properties of 58 malignant breast tumors determined by broadband diffuse optical spectroscopy. *Journal of biomedical optics.* 2006;11(4):044005.
27. Wang J, Geng YJ, Guo B, et al. Near-infrared spectroscopic characterization of human advanced atherosclerotic plaques. *Journal of the American College of Cardiology.* 2002;39(8):1305-1313.
28. Heimbach DM, Afromowitz MA, Engrav LH, Marvin JA, Perry B. Burn depth estimation--man or machine. *The Journal of trauma.* 1984;24(5):373-378.
29. Devgan L, Bhat S, Aylward S, Spence RJ. Modalities for the assessment of burn wound depth. *Journal of burns and wounds.* 2006;5:e2.
30. Hoeksema H, Van de Sijpe K, Tondu T, et al. Accuracy of early burn depth assessment by laser Doppler imaging on different days post burn. *Burns : journal of the International Society for Burn Injuries.* 2009;35(1):36-45.
31. Cross KM, Leonardi L, Gomez M, et al. Noninvasive measurement of edema in partial thickness burn wounds. *Journal of burn care & research : official publication of the American Burn Association.* 2009;30(5):807-817.
32. Sullivan TP, Eaglstein WH, Davis SC, Mertz P. The pig as a model for human wound healing. *Wound repair and regeneration : official publication of the Wound Healing Society [and] the European Tissue Repair Society.* 2001;9(2):66-76.

FIGURE LEGENDS

Figure 1.

SWIR spectrum encompasses excitation frequencies of endogenous cutaneous chromophores. (**A**) Short Wave Infrared (SWIR), defined here between about 1000 nm and 2500 nm, lies in the region between visible-near infrared (VIS-NIR) and Medium Wave Infrared (MWIR) encompassing the most specific wavelength marker for water spectroscopy, 1940 nm. (**B**) Viable and burned human skin (left) and schematic of SWIR reflectance from these regions (right). In viable skin that is well hydrated (top), increased water content is postulated to preferentially attenuate the reflectance of the 1940 nm wavelength compared to the 2250, 1650 nm or 1200 nm. However, in full dermis thickness burns (bottom), damage to vasculature and sebaceous glands renders the tissue less hydrated with proposed increased reflectance intensity across the SWIR spectrum.

Figure 2.

Basic SWIR imaging characteristics. (**A**) Imaging setups. In Epi-illumination configuration (left) the light source and the camera are on the same side of specimen and the light transverses twice the agar slab. In the Trans-illumination configuration the light transverses only once the agar slab. In both configurations the light intensity at the camera depends on absorbance and scattering of the light along its path, however air-agar surface scattering doesn't depend on the agar slab thickness. (**B**) Absorption Fraction vs. agar slab thicknesses for 1200, 1659, 1940 and 2250 nm light. Apart from light at 1940 nm which is fully absorbed by slabs 1 mm or more thick, the

absorbance of other wavelengths is greater in the Epi-illumination (left) than in the Trans-illumination (right) configuration, but is sensitive to the slab thickness at least up to 5 mm thick.

Figure 3.

SWIR light reflectance detects moisture levels in biologic tissue. (**A)** As baseline, 50 µL distilled water was applied on 4 inert substrate surfaces (P8 Grade filter paper, Fisher Scientific) and imaged with the Xeva-2.35-320 camera under collimated tungsten Epi-illumination at 1200, 1650 1940 and 2250 nm light. Top: Reflectance images normalized to no-substrate reflectance show attenuated reflectance in wetted regions at center for all wavelengths. Dark bands in wetted regions result from wrinkles. Bottom: Reflectance normalized to dry regions along red line in images. Reflectance fraction is visibly least attenuated for 1200 nm and most attenuated at 1940 nm (about 50% of dry regions). (**B**) An inert substrate (Kimwipe) was imaged with the 1940 nm filter on the camera under tungsten Epi-illumination before and after application of 30 µL water. Significant signal attenuation is present within the wetted region demarcated by red dashed line. SWIR reflectance at 1940 nm demonstrates diminished reflectance after water application (1382±369 vs. 747±249 ADU, $p<0.0001$). (**C**) SWIR reflectance images at 1940 nm of mouse skin under normal conditions and after administration of 10, 20, 30 µL of water, demonstrating progressive decrements of signal reflectance with increasing water administration. (**D**) SWIR reflectance at 1940 nm demonstrating diminished signal of dry depilated dorsum of mouse at progressive administrations of 10, 20, and 30 µL of water (794±83 vs. 444±73, 334±90, 235±43 ADU, $p< 0.001$). N=3 mice/group. $p<0.05$ demarcated by asterisk.

Figure 4.

SWIR reflectance can delineate superficial and deep burns in a porcine burn model: (**A**) In a porcine thermal injury model, a heated block delivered heat in 5×5-cm regions for short (S) and long (L) durations. Picture illustrates 8 regions in a sample animal under ambient visual light imaging. Unburned regions in between burns were used as controls. **(B**) SWIR images from sample animal with long (top) and short (bottom) duration heated regions with surrounding unburned areas. The heated regions (pink and red arrows) and sample biopsies regions (green arrows) are indicated. (**C**) Images showing processing outcomes for short (top) and long (middle) burns images whereby images from Panel B at 1650 and 2250 nm were summed and then divided by the corresponding 1940 nm images. The higher brightness in the long vs. short burn areas is corroborated by a bright area in the difference image (L – S, bottom). Difference is reduced in the top of the heated regions where skin surface is far from normal to the optical axis. (**D**) Collective analysis of SWIR images taken for each burn site (N=5 pigs, n=17 regions/group). Graph shows mean±SE of SWIR reflectance fraction of intensity of unburned (blue), short (pink) and long (red) burn regions, respectively, at: 1200 nm (0.3562±0.0146, 0.3925±0.0187, 0.4079±0.0155), 1650 nm (0.1884±0.0102, 0.18±0.011, 0.2347±0.0179), 1940 nm (0.111±0.0089, 0.12±0.0074, 0.1348±0.0145) and 2250 nm (0.3741±0.0146, 0.363±0.13, 0.42±0.0204). Asterisks indicate $p<0.05$. (**E**) Sample micrographs of biopsy sections from short and long burn regions (top) and cumulative analysis (bottom). White-dotted lines on standard H&E stained micrographs demarcate burned vs. normal dermis. White-dotted lines on Picrosirius (Pic) red stains corroborated burn

boundaries by highlighting changes to collagen ultrastructure. White arrows = depth from epidermis. Scale bars = 100 μm. Manual segmentations by three blinded analyzers averaged each individual specimen and show short burn resulted in burn depth of 590±57 μm vs. a long burn resulted in burn depth of 922±72 μm ($p=0.0002$, triple asterisks). N=5 pigs, n=10 specimen/group.

Figure 1

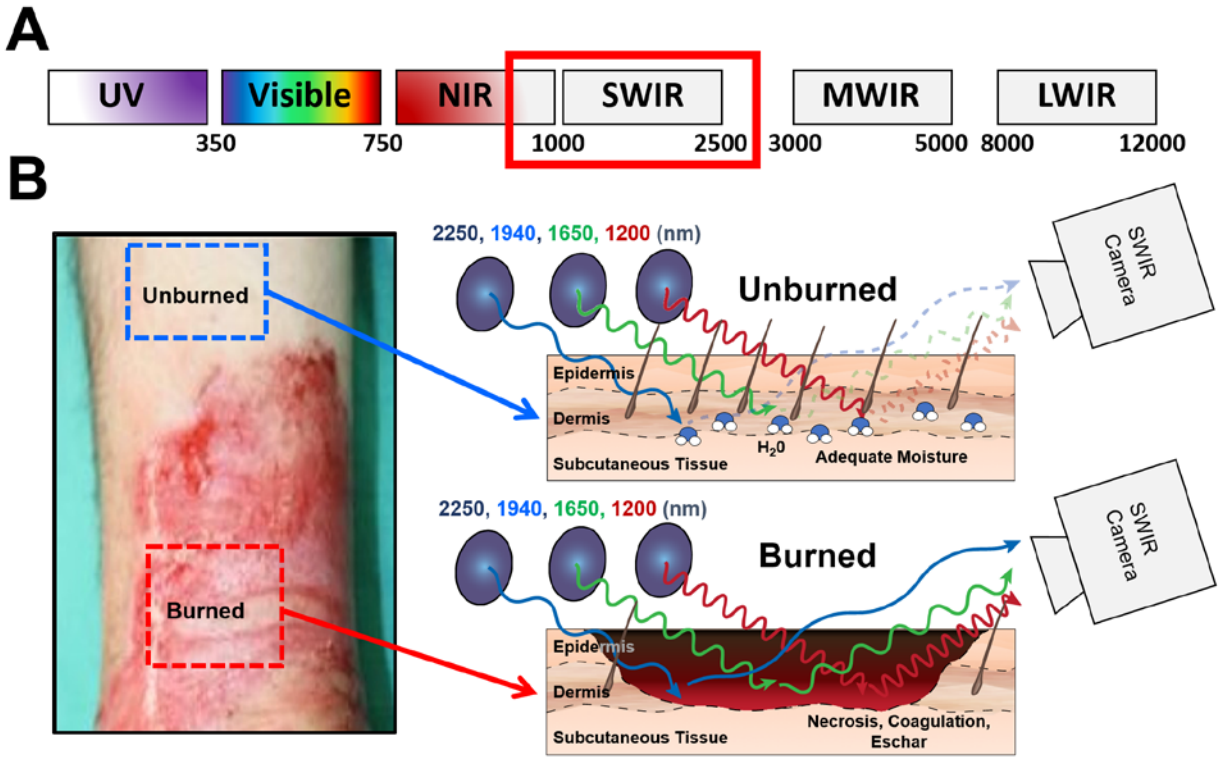

Figure 2

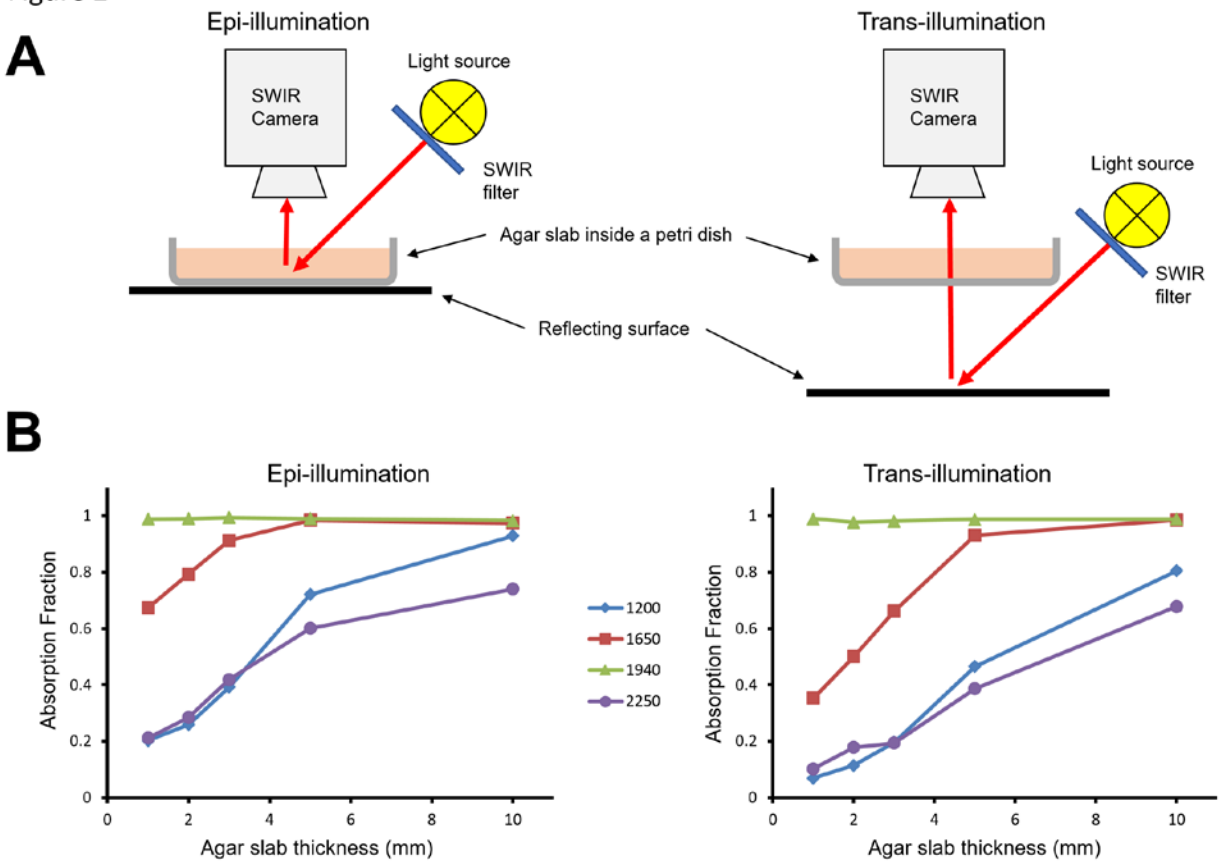

Figure 3

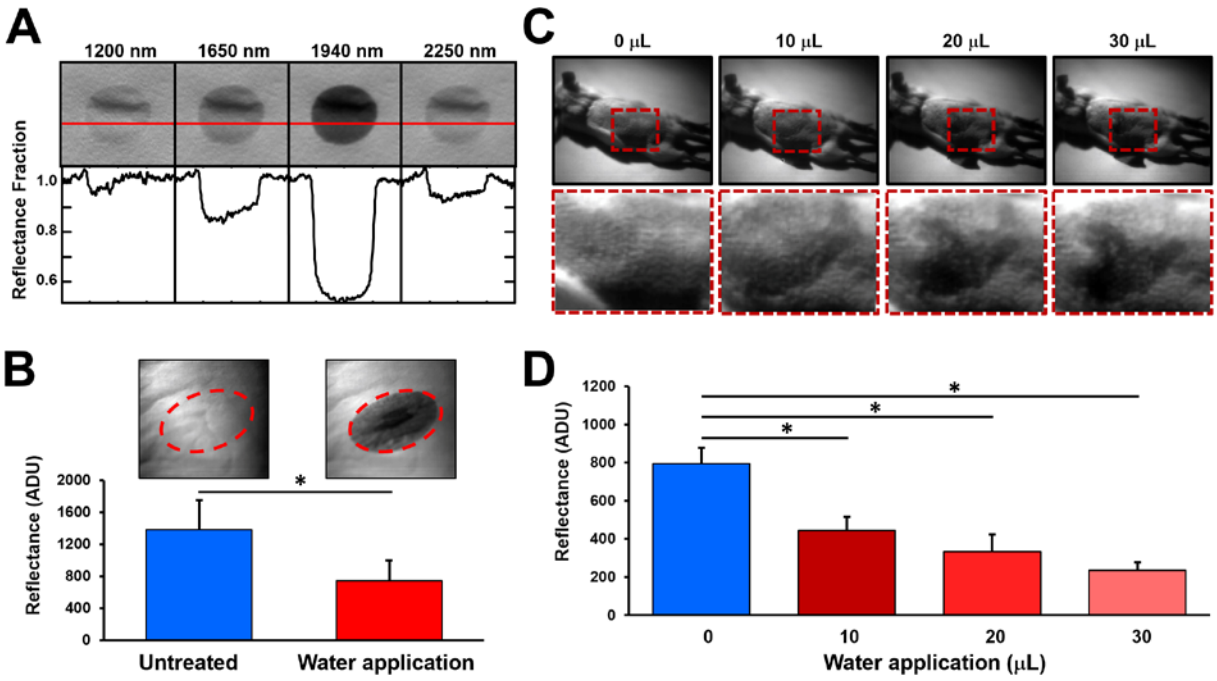

Figure 4

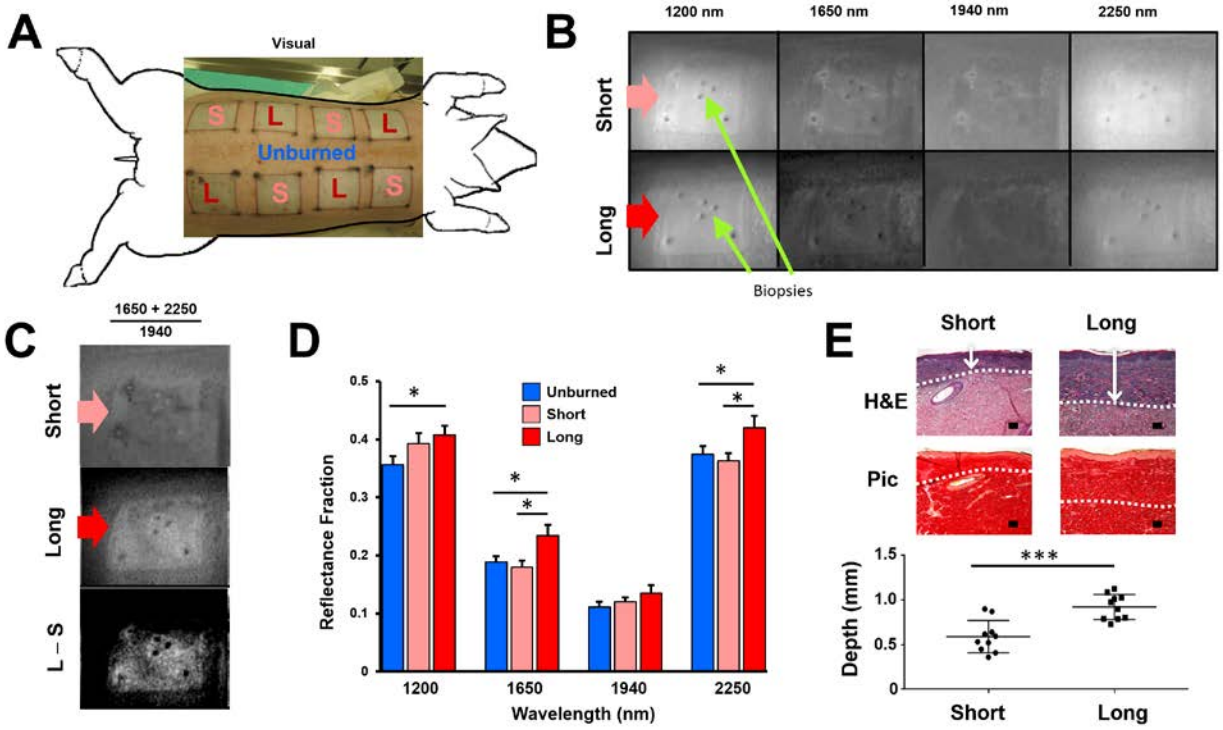

Figure 1

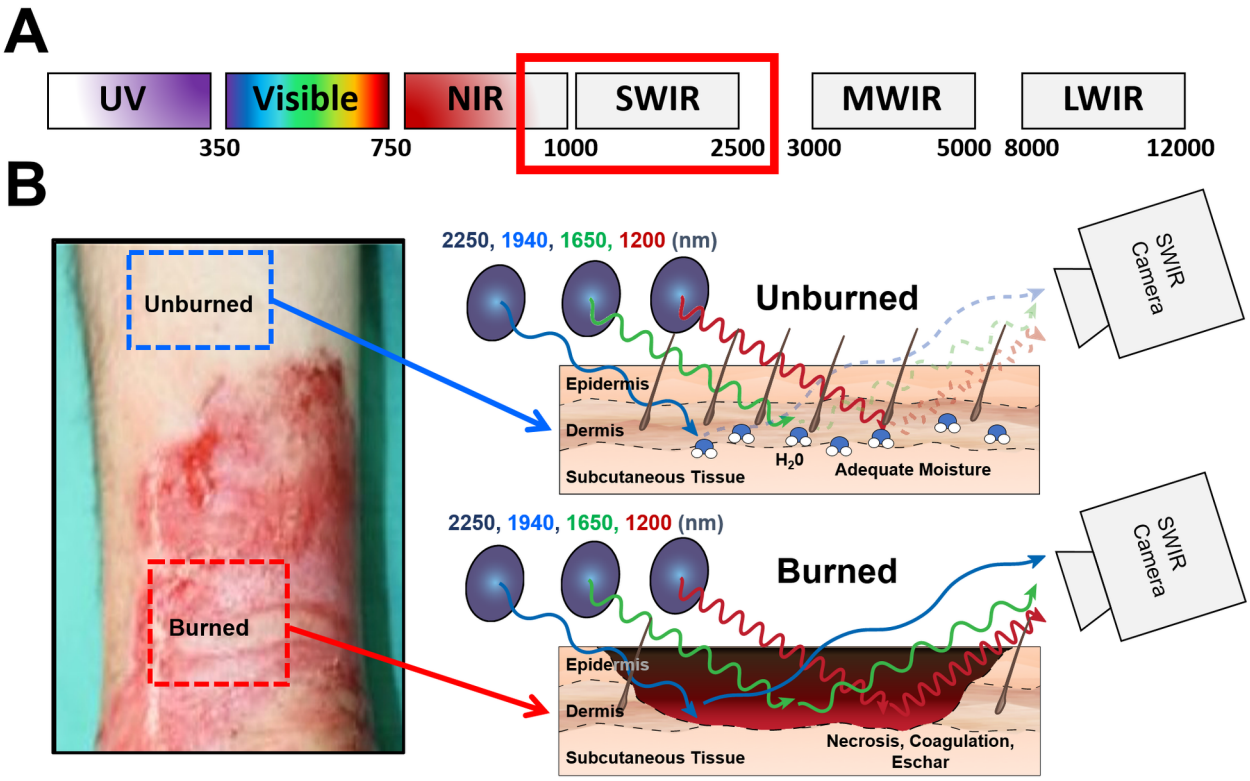

WRR_12779_Fig1.tif

Figure 2

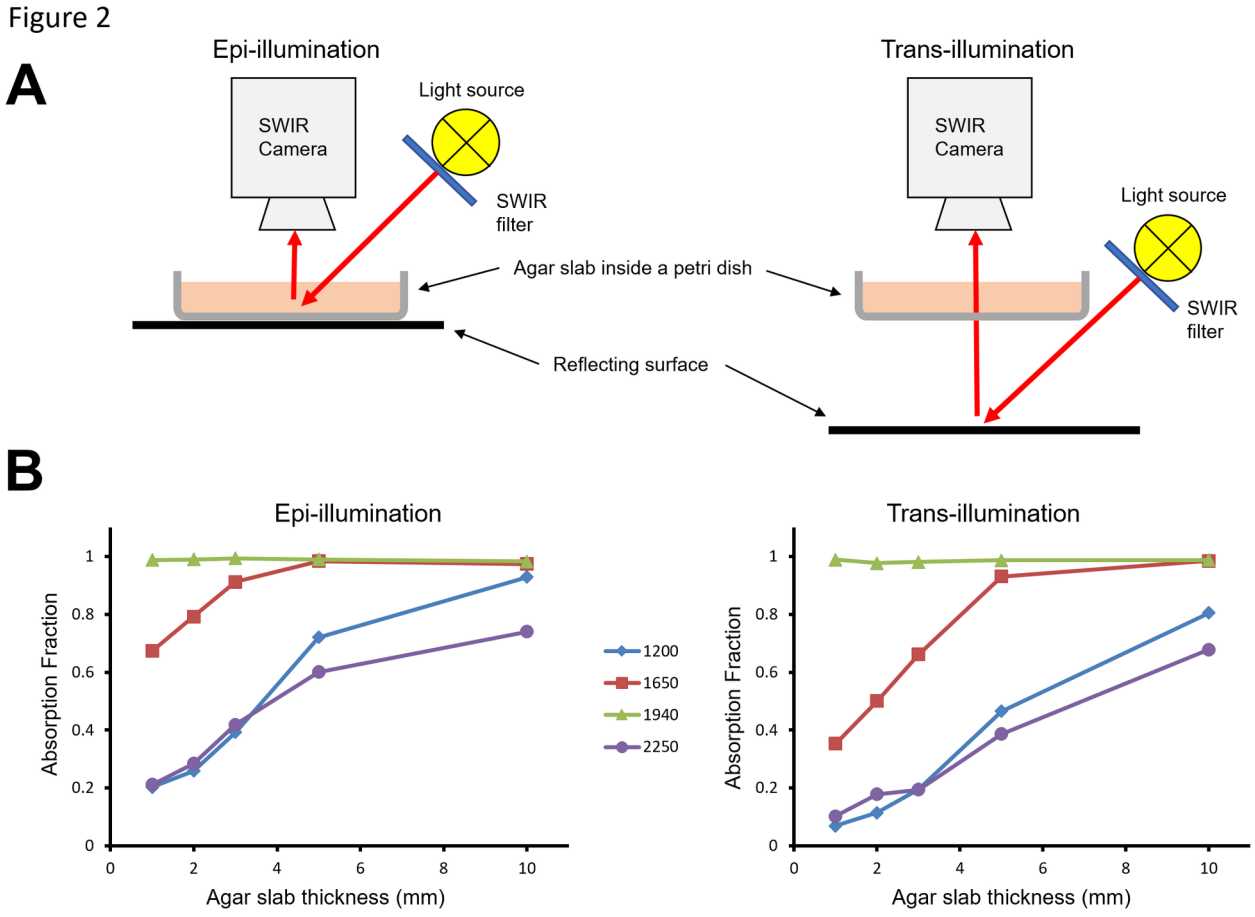

WRR_12779_Fig2.tif

Figure 3

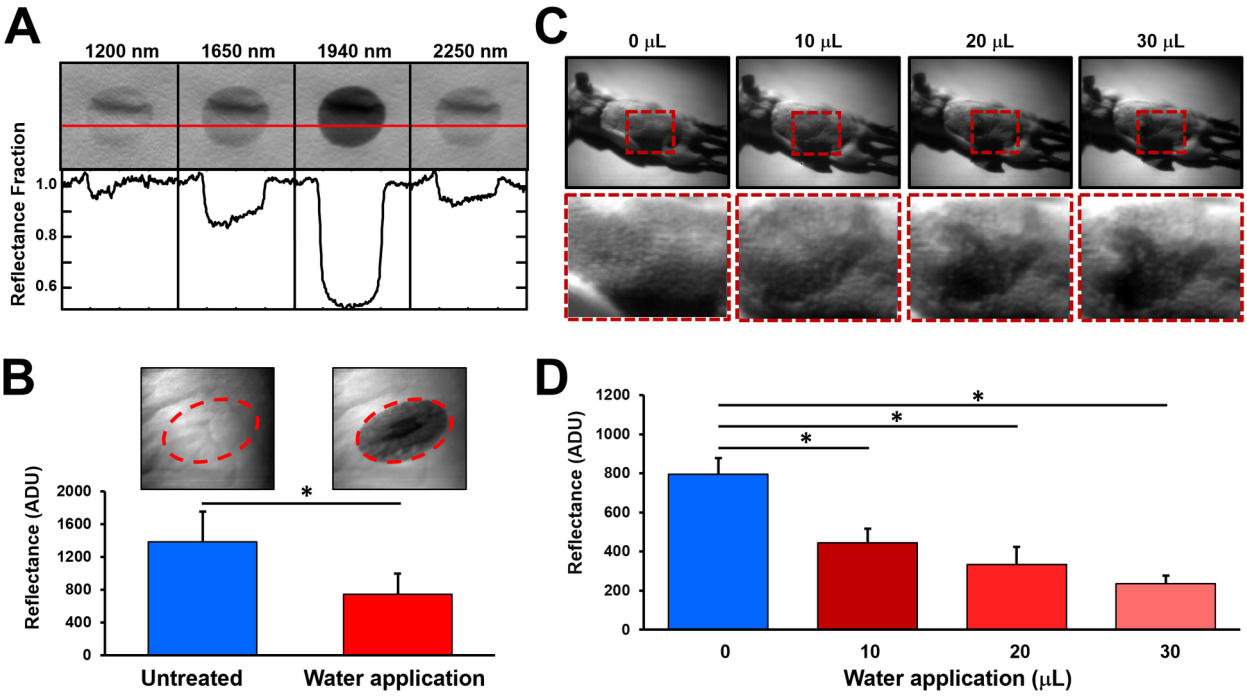

WRR_12779_Fig3.tif

Figure 4

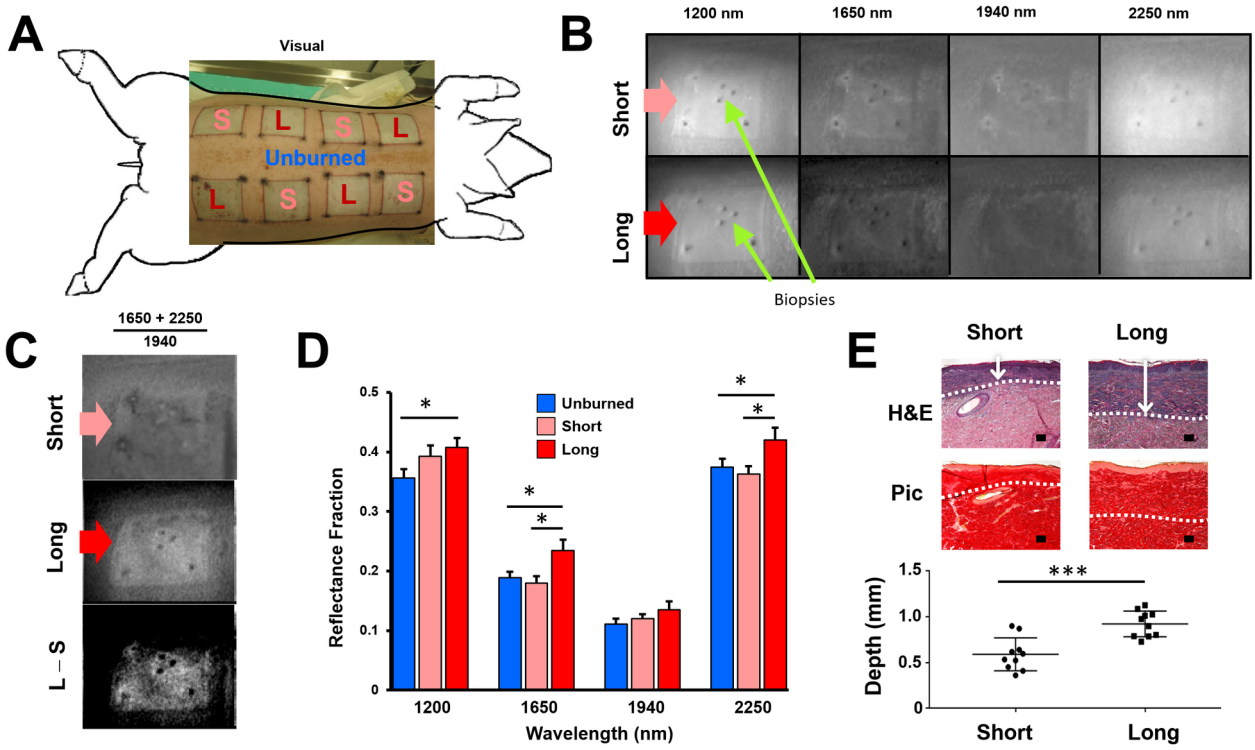

WRR_12779_Fig4.tif